Generalized spectral light scatter models of diverse bacterial colony morphologies

Iyll-Joon Doh[1], Jennifer Sturgis[2], Diana Vanessa Sarria Zuniga[3], Robert E. Pruitt[3], J. Paul Robinson[2,4], and Euiwon Bae[1,*]

[1]Applied Optics Laboratory, School of Mechanical Engineering; [2]Basic Medical Sciences, College of Veterinary Medicine; [3]Botany and Plant Pathology; [4]Weldon School of Biomedical Engineering, Purdue University, West Lafayette, IN 47907, USA

*Corresponding author: ebae@purdue.edu

ABSTRACT

An optical forward-scatter model was generalized to encompass the diverse nature of bacterial colony morphologies and the spectral information. According to the model, the colony shape and the wavelength of incident light significantly affect the characteristics of a forward elastic-light-scattering pattern. To study the relationship between the colony morphology and the scattering pattern, 3-dimensional colony models were generated in various morphologies. The propagation of light passing through the colony model was then simulated. In validation of the theoretical modeling, the scattering patterns of three bacterial genera, *Staphylococcus*, *Exiguobacterium*, and *Bacillus*, which grow into colonies having convex, crateriform, and flat elevations, respectively, were qualitatively compared to the simulated scattering patterns. The strong correlations observed between simulated and experimental patterns validated the scatter model. In addition, spectral effect on the scattering pattern was studied using the scatter model, and experimentally investigated using *Staphylococcus*, whose colony has circular form and convex elevation. Both simulation and experiment showed that changes in wavelength affected the overall pattern size and the number of rings.

Keywords: bacterial colony morphology, diffraction, light scattering, multi wavelength, spectral measurement

1. INTRODUCTION

This article has been accepted for publication and undergone full peer review but has not been through the copyediting, typesetting, pagination and proofreading process which may lead to differences between this version and the Version of Record. Please cite this article as doi: 10.1002/jbio.201900149

Bacterial Rapid Detection using Optical scattering Technology (BARDOT) applies an elastic light scattering (ELS) phenomenon to detect and classify microbial organisms. The innovative technology has shown promising results and potential applications in various bioscience-related areas [1–3]. BARDOT using a single-wavelength laser has been examined for a variety of genera or species of microbial organisms and provides promising classification power [4–10]. However, the single-wavelength model has a limitation in classifying organisms at lower hierarchical levels [11,12]. For several years, researchers have worked on developing innovative BARDOT approaches, resulting in the introduction of multispectral and reflective BARDOT instruments [13,14].

To study the theoretical background of the ELS technique, an optical forward-scatter model based on scalar diffraction theory was established in *Bae et al* [15]. Follow-up studies performed to expand the application of the scatter model have shown promising results in describing the nature of the forward light-scattering pattern produced from a bacterial colony. According to the model, the scattering pattern is a function of the morphological structure of the colony, including the colony height, diameter, and refractive index [14,16]. *Bae et al.* demonstrated that the size of the pattern is dependent on the aspect ratio of a bacterial colony – the ratio of a colony's center elevation to its diameter [16]. A Gaussian profile was used in previous studies to model the bacterial colony; it had an excellent fit for colonies having circular forms and convex elevations [16–18]. *Kim et al* explored laser-induced speckle scatter patterns produced from colonies with irregular elevation profile [19]. However, many other types of microorganisms have colonies that grow in different forms, elevations, and marginal shapes depending on their species, environmental conditions, and sometimes their virulence or antimicrobial susceptibility [5,20,21].

Environmental stress causes organisms to produce mutations, which are often recognized by their variations in colony morphology. Small colony variants (SCVs) come from mutations of metabolic genes that cause the colonies to grow slowly and produce distinctive phenotypic and pathogenic characteristics [22]. Owing to the slow growth rate, the SCV forms colonies of smaller size. More morphological variations as a result of virulence gene–associated mutants are

reported in *Simpson et al* [23]. Both opaque and translucent colonies were observed in virulent strains of *Vibrio vulnificus*, indicating variations in colony opacity due to the mutation. It is clinically important to study the variants because not only the phenotypic but also the pathogenic traits change. For example, SCV bacteria are known to be more persistent, recurrent, and antibiotic-resistant compared to regular types of bacteria [24]. In addition, it was reported that both colony morphology and virulence are correlated with the production of capsular saccharide that helps the antibiotic resistance [25]. The correlation between the colony morphology and light-scattering signal needs to be thoroughly investigated in order to study the effect on light-scatter patterns of gene manipulation of a bacterial colony [26]. Therefore, extended study of the optical scatter model with respect to a variety of colony shapes is needed to encompass the diverse nature of bacterial colony growth.

The multispectral BARODT utilizes 405-, 635-, and 904-nm lasers to generate forward light-scattering patterns at three different wavelengths. The multispectral approach selects optimal features from each wavelength component and delivers enhanced classification power compared to a single-wavelength instrument [13]. The improved performance from an increased number of wavelengths encourages potential utilization of even more wavelengths. The effect of spectral variation on the light-scatter pattern is discussed in *Kim et al* [17]. The authors measured three spectral light-scatter patterns from *Staphylococcus aureus* in a colony and compared them to the predicted patterns. The predictions well illustrated the relationship between the wavelength and the pattern shape, although only three wavelengths were involved.

This paper reports an extended study of the optical scatter model to explore the effect of two factors on the forward light-scatter patterns: 1) the morphology of a bacterial colony and 2) the wavelength of the incident laser beam. The 3-dimensional colony models were generated based on common shapes of bacterial colonies and then employed to predict the light-scatter patterns. The predicted patterns were experimentally checked against patterns yielded from colonies of various shapes. To study the spectral effect, the scatter patterns at a series of wavelengths were simulated using the scatter model.

2. MATERIALS AND METHODS

2.1 Theoretical Modeling

2.1.1 Optical scatter model

The coordinate system for the optical scatter model is presented in Figure 1(A). The bacterial colony is located at the aperture plane and the light-scatter pattern is captured.at the imaging plane. The scatter model was derived based on a scalar diffraction theory with the Huygen-Fresnel Principle and Fresnel approximation; derivation steps can be found in *Bae et al* [15]. The electric field at the imaging plane is expressed as Eq. 1:

$$E_i(x_i, y_i) \approx C\iint \mathrm{T}(x_a, y_a)\exp\left[ik\Phi_{overall}(x_a, y_a)\right]\times\exp\left[-2\pi i(f_x x_a + f_y y_a)\right]dx_a dy_a \quad (1)$$

where (x_a, y_a) and (x_i, y_i) are the coordinates on the aperture and imaging planes, respectively; C is the proportionality constant; k is the wave number; f_x and f_y are the spatial frequencies. The equation is grouped into two major components, amplitude modulator and phase modulator. The amplitude modulator, $\mathrm{T}(x_a, y_a)$, is a term that is highly related to the intensity of the scatter pattern, whereas the phase modulator, $\Phi_{overall}(x_a, y_a)$, mainly affects the shape or the size of the pattern. The amplitude modulator is defined by Eq. 2:

$$\mathrm{T}(x_a, y_a) = t(x_a, y_a)\exp\left[-\frac{\left(x_a^2 + y_a^2\right)}{w^2\left(z_a\right)}\right] \quad (2)$$

where $t(x_a, y_a)$ denotes the 2-D transmission coefficient that includes the colony profile term to consider the inter-bacterium reflection along the thickness of the colony[16] and $w(z_a)$ is the beam waist in the aperture plane. The phase modulator is a summation of three components, colony (Eq. 4), quadric (Eq. 5), and radial phase (Eq. 6). z_i is the distance between aperture and imaging plane, and R is the radius of the wavefront in the aperture plane. The colony phase component is expressed as a function of the colony profile, $H(x_a, y_a)$, since it is governed by the

optical path-length term, indicating that the overall phase component is relevant to the shape of the colony.

$$\Phi_{overall} = \Phi_c + \Phi_q + \Phi_r \tag{3}$$

$$\Phi_c(x_a, y_a) = (n_{bac} - 1)H(x_a, y_a) \tag{4}$$

$$\Phi_q(x_a, y_a) = \frac{(x_a{}^2 + y_a{}^2)}{2z_i} \tag{5}$$

$$\Phi_r(x_a, y_a) = \frac{(x_a{}^2 + y_a{}^2)}{2R} \tag{6}$$

Because both amplitude and phase components of the scatter model contain the colony profile term, the intensity and shape of the light-scattering pattern is affected by the morphology of a bacterial colony.

Furthermore, the scatter model can be expressed as function of wavelength since multiple terms are physically related to the wavelength of the incident beam. For example, terms like wavenumber, beam waist, and refractive indices in both amplitude and phase modulators have direct relationship to the wavelength. Not only that, the spatial frequencies are also dependent on the wavelength. A detailed explanation of the relationship can be found in *Kim et al* [17].

2.1.2 Colony profile generation

To study the morphological effect on light-scatter pattern, 3-D bacterial colony models were built based on common colony shapes. The colony model was assumed to be a spatial modulator that affects the amplitude and phase of the incident light wave [16]. The shape of a bacterial colony is described in terms of form, elevation, margin, texture, size, and color [27]. In this paper, only the effect of the form and elevation were studied, neglecting the others. Form is defined as a basic shape observed from the top view, and elevation describes the view from the side of a colony. Colonies with circular forms were the main subjects of investigation, in combination with convex, flat, umbonate, and crateriform elevation. As illustrated in Figure 1(A), the origin for the colony model was located at the aperture plane, considered to be the surface of agar, and

the elevation was defined in the positive z-direction. The agar surface was assumed to be flat, and therefore the height outside the colony boundary was fixed at 0. As described in Figures. 1(B) and (C), a colony with convex elevation was modeled using a Gaussian profile with tailing edge (Eq. 7) and an effective radius (Eq. 8) [16,17].

$$H(x_a, y_a) = H_0 \exp\left[-\frac{(x_a^2 + y_a^2)}{r_c^2} \right] \tag{7}$$

$\mathrm{H}(x_a, y_a)$ is the colony profile as a function of (x_a, y_a), the 2-D aperture coordinate. H_0 is the center height and r_c is the effective radius of the colony, defined as

$$r_c = \frac{D}{2F} \tag{8}$$

where D is the target diameter of the colony, and F is a factor (1.6) to render a $1/e^3$ radius [16]. For the flat colony, the elevation within the colony boundary was fixed to H_0 (Eq. 9).

$$H(x_a, y_a) = H_0 \tag{9}$$

In contrast to the first two elevation types, umbonate and crateriform elevations have more complicated profiles. The umbonate elevation, which has a bump at the center, was generated by combining half ellipsoid and Gaussian profiles (Eq. 10).

$$H(x_a, y_a) = \begin{cases} H_0 \exp\left[-\frac{(x_a^2 + y_a^2)}{r_c^2} \right], & \text{if } (x_a^2 + y_a^2) \le \left(\frac{r_c}{2} \right)^2 \\ \sqrt{\frac{H_0}{2}^2 \left(1 - \left(\frac{x_a}{r_c} \right)^2 - \left(\frac{y_a}{r_c} \right)^2 \right)}, & \text{if } (x_a^2 + y_a^2) \ge \left(\frac{r_c}{2} \right)^2 \end{cases} \tag{10}$$

The Gaussian profile was designed to be the bump and combined with a half ellipsoid. The crateriform elevation has a crater at the center, and a radial wave function was applied to design the unique profile (Eq. 11).

$$H(x_a, y_a) = \frac{H_0}{2} \sin(\alpha \, (x_a^2 + y_a^2) + \beta) + \frac{H_0}{2} \tag{11}$$

H_0 was no longer the center elevation since the center was depressed. But it was still the maximum height of the colony. The radial wave function, as shown in Eq. 11, has two constants, α and β, which alter the diameter and crater depth of the colony. These two values were iteratively optimized.

2.2 Experiment

2.2.1 Sample preparation

Bacillus and *Exiguobacterium* were cultured on plate count agar (PCA), and *Staphylococcus* was prepared on trypticase soy agar (TSA) (Bacto™, BD Diagnostics, Franklin Lakes, NJ). *Staphylococcus* was obtained from a frozen stock at -80 °C, streaked on TSA, and incubated at 37 °C until its colonies were found visually. The streaked plates for *Bacillus* and *Exigobactium* were similarly prepared, but incubated at 30 °C. For each genus, one colony was randomly picked, scooped from the streaked plate, and diluted serially in 4 ml buffer solution (PBS) three times by a factor of 1:40. A 50-µl aliquot of the last dilution tube was spread on TSA or PCA depending on the genus. *Staphylococcus* was incubated at 37°C and the others at 24 °C until the diameter of colony reached about 800 to 1000 µm. The species name for *Staphylococcus* and *Exiguobacterium* were *Staphylococcus aureus* and *Exiguobacterium undae*. The species name of *Bacillus* was unknown since the identification process was performed with lower resolution. It was identified to one of 8 species in *Bacillus*, which were *B. cereus, B. wiedmannii, B. pacificus, B. mobilis, B. paranthracis, B. proteolyticus, B. toyonensis, and B. thuringiensis*.

2.2.2 Morphological analysis

The 1-D cross-section of a colony profile was acquired using an integrated colony morphology analyzer (ICMA) [28]. This instrument utilizes a laser confocal displacement meter (LT9010M, Keyence, New Jersey) which uses a 655-nm laser source to collect reflectance from the colony. The collected data were then visualized in MATLAB.

An inverted microscope (Nikon Eclipse TE2000-U, Nikon Corp., Tokyo, Japan) equipped with a confocal imaging system (Radiance 2100MP, Bio-Rad Laboratories, Inc., Hercules, CA) was utilized to measure the colony profile in higher resolution. A 10× objective lens with NA of 0.5 (CFI Super Fluor 10×, Nikon Corp., Tokyo, Japan) was mounted on the confocal microscope. The resolution of the image was 512 × 512 × 192 pixels, and each pixel size was 2.36 μm × 2.36 μm × 2.36 μm. The obtained stackable images were reconstructed to a single 3-D image using the open-source image-processing program ImageJ. The 1-D cross-section across the center of the colony was visualized by the orthogonal-view function in the software.

2.2.3 ELS pattern measurement

A collimated 635-nm laser (Coherent 0221-698-01 REV B, Coherent Inc., Santa Clara, California) was utilized to generate a single-wavelength forward-scatter pattern. The beam diameter was 1.1 mm and the power 0.95 W. To capture the scatter pattern, a monochromatic complementary metal-oxide semiconductor (CMOS) sensor (PL-B471, Pixelink, Ottowa, ON, Canada) was placed below the petri dish. The resolution of the sensor is 1280 × 1024 pixels with 6.7-μm unit pixel size.

For the spectral analysis, BARDOT with multiple spectra lines were constructed. The major components of this version of BARDOT are a white-light laser, an AOTF, and a CMOS sensor. The white-light laser, also known as a supercontinuum laser (SC-5, YSL Photonics, Hubei, China), provides a wavelength range of 470 – 2400 nm. The AOTF crystal block (MIM-200, Brimrose Corp., Sparks Glencoe, MD) was positioned after the laser to select a specific wavelength of interest. The filter was controlled by its own driver (VFI-139-90-SPS-A-C2, Brimrose Corp., Sparks Glencoe, MD) that generates an acoustic signal from 95 to 180 MHz, equivalent to 450 – 750 nm in wavelength. The CMOS sensor was placed below the petri dish to capture the scatter pattern.

3. RESULTS AND DISCUSSION

3.1 ELS Pattern Prediction

The mathematically generated colony models and their simulated forward-scatter patterns are presented in Figure 2. The first row displays the colony models in isometric view, the second shows the corresponding simulated patterns. The overall height and diameter of the colony model were fixed to 0.08 and 1 mm respectively in order to keep the aspect ratio of the colony model to 0.08. In this study, the colony with crateriform elevation was treated as an exception. The center elevations of the other colonies are equal to the overall heights. Since the colony with crateriform elevation has a crater that makes a difference between center and overall heights, the ratio of overall height to diameter was treated as the aspect ratio. *Kim et al.* reported that the aspect ratio ranged from 0.07 to 0.2, determined by the bacteria species or the incubation time [28]. The aspect ratio decides the overall size and the number of rings within the pattern. Thus, we chose a smaller number for the aspect ratio and kept the same for all models. In addition, optical parameters like refractive index of the cell, wavelength, and beam waist were fixed throughout the simulation to focus on the effect of morphological variation. The refractive index of a bacteria cell was set to 1.4686, assuming it as a thin cellulous film [17]. The wavelength and the beam waist were fixed at 635 nm and 1 mm, respectively. As a result, each colony model produced a unique pattern shape. The colony model in Figure 2(A) had convex elevation, and the pattern had clear circular rings uniformly distributed. The result agrees with previous works where the scatter pattern was simulated using a colony model with Gaussian profile [16,17]. For the crateriform colony model, the crater depth was set to half the overall height of the colony. A pattern of circular rings was also observed, but two different-sized patterns overlapped at the center. Because the overall size of the pattern was much larger than in the other cases, the pattern was scaled down by a factor of 2.5 and displayed in Figure 2(B). The larger pattern came from the ascending profile on the outer side of the colony, and the smaller from the crater. The colony model with umbonate elevation produced a pattern resembling the one in Figure 2(A), as a part of the profile was Gaussian. However, the inner part of the pattern was dimmer owing to the dissimilar profile on the outer part of the model. Since the model in Figure 2(D) had a flat

elevation that caused a sudden change of refractive index, only small diffraction rings were observed around the beam spot.

In Figure 2, we observed that only circular diffraction rings were generated regardless of the elevation type because the colony models shared the circular form. However, each type of elevation had a unique 1-D profile across the center; depending on the curvature, the number, location, and intensity of the rings were determined. In Figure 2(C), we observed that the outer part of the colony model majorly contributed to the interior shape the pattern. To understand which part of the colony contributes to which part of the pattern, a theoretical study using the scatter model was conducted. An arbitrary shape other than a circle was integrated to show how the new shape affected the pattern by its location. There were two different sets of simulations: one had a colony model with a star-shaped form shrinking towards the center; the other had a star-shaped hole at the center expanding out to the edge. To effectively show the impact of the new form and its boundary location on the colony profile, the contrast was maximized by making either side of the boundary zero. In Figure 3, the simulation results show that various sizes of star-shaped forms and holes affected the shape of the pattern differently. The second column in both Figure 3(A) and (B) represents a derivative of the phase component across the center of the colony model, which indicates the slope of the 1-D profile. The maxima and minima of the plot represent the maximum slope of the profile on each side of the colony model. In Figure 3(A), when the shape on the edge of the colony was modified, some spokes were created on the inside of the pattern. When the star began to interfere with the shape at the maximum slope, the outermost ring was no long a plain circle, but became a ring with spikes. In addition, because the area outside the form was completely flat, the intensities of the rings inside were very weak. In contrast, in both Figure 3(A) and (B), the patterns were completely circular when there was no interference with the forms at the maximum slope. In Figure 3(B), the smallest star-shaped hole created waves on the rings, and as this hole was expanded, the rings started to disappear and only spokes remained. The observation implies that the shape of forms and the location of their

boundary on the colony profile determines the shape of rings and spoke pattern; the outer part of the colony contributes to the intensity of the rings, and the inner part determines their shape.

3.2 Experimental Verification

3.2.1 Morphological analysis

Colonies of *Bacillus*, *Exiguobacterium*, and *Staphylococcus* are categorized into three sets: colonies with convex, crateriform, or flat elevation. For each bacterium, the morphological data were measured with three different modalities; representative images are presented in Figure 4. A plate image was taken by a smartphone camera (top left); a single colony was magnified by a stereo microscope (top right); 1-D cross-section profile was measured by ICMA (bottom left). According to the stereo microscope images, the colonies in Figure 4(A) and (B) have uniform and circular forms, whereas the colony in Figure 4(C) has an irregular form. The 1-D profiles clearly show that each bacterial colony has convex, crateriform, or flat elevation, but they differed slightly from the models discussed in Figure 2. Therefore, new 3-D colony models reflecting the morphological information collected by the aforementioned techniques were designed (bottom right). The aspect ratio of each colony was calculated based on 1-D profile data: 0.12, 0.068, and 0.035 for *Staphylococcus*, *Exiguobacterium*, and *Bacillus*, respectively. Accordingly, the ratios of the new colony models were assigned to 0.1, 0.05, and 0.02 with fixed colony diameter of 1 mm. The crater depth in an *Exiguobacterium* colony was not as deep as the model in Figure 2, and therefore it was reduced to 20% of the overall height.

Using a higher-resolution confocal microscope, 3-D images were collected for more precise analysis of the colony morphology. A total of 192 stackable confocal images were captured, started at 400 μm above and finished at 50 μm below the agar surface, with a 2.36-μm interval between images. The collected images were projected to a single image; the representative images are shown in Figure 5. For a projected image, the cross-sections across the center of a colony in the vertical and horizontal directions were attached on the right and bottom. Compared to stereo-microscope images, the projected images showed better quality in illustrating the flat

colony. The colonies in Figures 5(A) and (B) were not clearly measured owing to the steep slopes of the profiles that caused difficulty in capturing reflectance from the colony surface with the given numerical aperture of the mounted objective lens. This problem also arises in the cross-section images. Meanwhile, the colony in Figure 5(C) had a small aspect ratio, and therefore the projected image was clear and provided detailed morphological information. Because the colony of *Bacillus* was relatively more transparent than the other two, the shape was not able to be clearly identified in the stereo-microscope image provided in Figure 4(C). Conversely, the projected image in Figure 5(C) well illustrated the form and surface roughness. The colony profiles in the cross-sections were less exaggerated than the profiles in Figure 4 owing to the different pixel size. A similar observation was made in Figure 5 that *Staphylococcus* in a colony had the highest aspect ratio, followed by *Exiguobacterium*, and then *Bacillus*. Based on the confocal image, the surface of a *Bacillus* colony displayed bumpy and irregular surface structure although the *Bacillus* colony was considered flat. Therefore, the flat-colony model was modified by applying a Gaussian random surface to imitate the irregularity.

3.2.2 Pattern analysis

Figure 6 is the comparison between the predicted and experimentally measured light-scatter patterns. Figures 6(A) to (C) represent the simulated patterns from the modified colony models having convex, crateriform, and flat elevations. Figures 6(D) to (F) are the experimentally captured patterns of *Staphylococcus*, *Exiguobacterium*, and *Bacillus* in colonies. Each of the simulated patterns had unique features that could be differentiated from one to another and that resulted from the distinctive colony morphology. The features were also noticed in the experiment patterns, indicating an excellent agreement between simulation and experiment.

A pattern with circular and concentric rings was predicted for a colony model with Gaussian profile, and a similar light-scatter pattern shape was produced from a *Staphylococcus* colony. In Figure 6(A), more rings were observed compared to the pattern in Figure 2(A), as the colony height was increased, and the number of rings is directly proportional to the colony height.

Figure 6(B) also had a pattern with circular rings, but a difference was noticed at the center. A bright circular band formed around the laser spot, which was also found in Figure 6(E). The band resulted from the crater of the colony, which was introduced as a smaller secondary pattern earlier in Figure 2(B). However, the decrease in the depth, resulting in the decrease in the slope, shrank the smaller pattern into a bright band. Unlike the first two types of colony elevation, the flat colony with irregular surface resulted in a pattern that is neither uniform nor symmetric. Figures 6(C) and (F) were alike in that no diffraction rings were observed, and both of the patterns had scattered light randomly spreading out from the center. This agrees to the result presented in *Kim et al*; scattered and speckled patterns were produced from colonies with irregular elevation profile [19]. The simulation well predicted the smallest pattern size for the flat colony which also had the smallest aspect ratio. The quantitative comparisons are presented in the supplementary section.

Unlike *Staphylococcus*, which had a clear circular pattern, the *Exigobacterium* pattern had spikes around the rings and observable spokes. However, in the simulation only smooth circular rings were generated. One possible reason is the surface roughness of the real colony. Although the 3-D colony model imitated major characteristics like form and elevation, minor characteristics like surface roughness were not considered. The stereo microscope images in Figure 4 show that the surface of a *Staphylococcus* colony looks smoother than that of an *Exiguobacterium* colony. According to the simulation result in Figure 3, the spikes were generated on the rings by the shape of the form on the slope. Therefore, the surface roughness of the colony can be exaggerated and portrayed in the scattering pattern. In addition, the effect can be explained by the internal structure of the colony. In this paper, we assumed the colony to be a composition of rectangular cells [16]. However, the internal structure is more complex than that, and cells also vary by species. Therefore, further investigation is required to study the effect of internal structure on the scatter pattern.

3.2.3 Crateriform elevation

The light-scatter pattern of the colony with crateriform elevation was further studied to explore the effect of its overall height and crater. The colony height and crater depth were varied from 0.02 to 0.06 mm and 10 to 50% of the overall height, respectively. The diameter of the colony was fixed at 1 mm. Qualitative comparison of the patterns predicted for colonies with various height and crater depth is presented in Figure 7. The simulation results demonstrate that the size of the pattern and the ring number of both inner and outer patterns were dependent on the two factors. The increase in the overall height indicated a steeper slope for the colony profile. The slope of the crater was also affected, since it was dependent on the overall height during the simulation. Therefore, the increase in the overall height of the colony generated a larger pattern with a greater number of rings in both inner and outer patterns. Similarly, changes in the crater depth affected not only the size of the pattern on the inside, but also the overall size of the pattern.

A similar result was observed in time-resolved light-scatter patterns of *Exiguobacterium* colonies (Figure 8). The 1-D profiles and the scattering patterns of *Exiguobacterium* were measured for 8 hours, beginning after initial growth period of 24 hours (t_0). The 1-D profile showed that, in general, the colony was growing in both vertical and horizontal directions, but vertical growth was slower than horizontal growth. At t_0, the crater was not observed, but over a longer time the center of the colony became depressed. As a result of the colony deformation, the overall size of the pattern was dramatically increased and the rings became unclear. On the other hand, the smaller pattern became obvious and was evolving from the center with an increasing number of rings.

Previous studies have reported the relationship between the aspect ratio and the half maximum diffraction angle, indicating the overall size of the pattern [16,28]. At the beginning of this paper, we considered the colony with crateriform elevation as an exception in measuring the aspect ratio. The aspect ratio was simply used to define the general slope of a convex colony in the literature; this is not applicable to colonies with crateriform elevations, since the center elevation no long defines the overall height of the colony. From time-resolved experiments, we observed that the whole pattern for *Exiguobacterium* increased in size over time. However,

because the diameter of the colony was growing faster than the vertical height, the overall height to diameter ratio was decreasing, contradicting the positive relationship argued in previous reports. The disagreement can be simply explained by the slope at the edge of the colony. Based on simulations and time-resolved experiments, we observed that the slope on the outer part of colony was dependent on the crater depth. Over time, the crater became deeper and expanded towards the edge of the colony. The horizontal expansion of the crater was faster than the expansion of colony diameter. Therefore, the outer part of colony was pushed out by the crater, resulting in a steeper slope and a larger pattern.

3.3 Spectral Analysis

The spectral effect on the forward-scatter pattern was investigated further with the optical forward-scatter model. We previously reported that multi-spectral BARDOT provided promising classification accuracy of over 93%, and showed that the wavelength of incident light had significant effect on the pattern by influencing the size, number of rings, and the gap between the rings [13,17]. As an extended study of multi-spectral analysis, we conducted another pattern simulation with respect to the wavelength, and increased the experimental wavelength by utilizing a white-light laser and an AOTF. In addition, a hyperspectral forward scatterometer–based bacterial phenotyping prototype was developed and tested on *Staphylococcus* to see the spectral effect on the scattering pattern. In Figure 9(A), experimentally captured forward-scatter patterns generated from a colony of *Staphylococcus* at various wavelengths are presented. In Fig 9 (B), 1-D cross-sections of experimental and simulated patterns of corresponding wavelength are illustrated. Based on the pixel resolution, the x-coordinates of the cross-section figures were converted from pixels to millimeters. As expected, the result showed that longer wavelengths produced smaller patterns and fewer number of rings. Although the number of maxima was not exactly equal, the result was clear that simulation well predicted the decreasing trend in diffraction angle for increased wavelength. For pattern size, the average percent error between theoretical and experimental results was 3.65%. Although data from only six wavelengths were

shown in this study, AOTF has the capability of dividing the visible spectrum into many wavelength data points, meaning that more wavelength data can be collected. This could potentially upgrade the accuracy of classification. Moreover, not only can the spectral pattern be obtained, but also hyperspectral image or absorption analysis can be performed to aid the classification.

4 CONCLUSION

Colony morphology can be thought of as a phenotypic expression of the genotypic characteristics of a microorganism. The morphology is described in terms of size, form, elevation, margin, surface, opacity, and color, and variation of these characteristics generates unique scattering patterns as light penetrates a colony. Since the shape of a scattering pattern depends on the biophysical characteristics of the colony, it is essential to study variation in colony morphology and its correlation to the resulting pattern. Therefore, the forward light-scatter patterns from a variety of bacterial colonies with distinctive shapes were studied using 3-D colony models and a scalar diffraction theory–based optical scatter model. For verification of the theoretical study, three bacterial genera, *Staphylococcus*, *Exiguobacterium*, and *Bacillus*, were chosen for comparison of their colony profile and scattering patterns to those of the simulations. Excellent agreement was observed between simulation and experiment. The spectral effect on the patterns was investigated, with results similar to those of the previous paper, that the size, ring number, and ring gaps are highly dependent on the wavelength of incoming light.

The validation process of the optical scatter model in this paper has demonstrated the behavior of light scatter pattern with respect to the colony shape or the wavelength of incident laser beam. Understanding the behavior is beneficial in microbial detection using light scattering technique because the mutation or virulence can affect the colony morphology, and this can be expressed in the scatter pattern. In addition, the model helps study the inverse problem of the scatter pattern to colony, and to biological activity. Moreover, this is helpful in developing

improved feature-based classification algorithm using unique features extracted from morphological or optical traits detected in the scatter pattern.

In future, for continuing evaluation of the optical scatter model, further studies on scattering patterns generated from colonies with complicated or non-symmetric morphology are required along with spectral analysis. Furthermore, predicting reflective scattering patterns introduced in reflective type BARDOT is another interesting topic to expand application of the theoretical model.

5 ACKNOWLEDGMENT

This material is based upon work supported by the U.S. Department of Agriculture, Agricultural Research Service, under Agreement No. 59-8072-6-001. Any opinions, findings, conclusions, or recommendations expressed in this publication are those of the author(s) and do not necessarily reflect the view of the U.S. Department of Agriculture.

6 REFERENCES

1. Banada, P.P., Guo, S., Bayraktar, B., Bae, E., Rajwa, B., Robinson, J.P., Hirleman, E.D., and Bhunia, A.K. *Biosens. Bioelectron.*, **22** (8), 1664–1671.
2. Banada, P.P., Huff, K., Bae, E., Rajwa, B., Aroonnual, A., Bayraktar, B., Adil, A., Robinson, J.P., Hirleman, E.D., and Bhunia, A.K. (2009) Label-free detection of multiple bacterial pathogens using light-scattering sensor. *Biosens. Bioelectron.*, **24** (6), 1685–1692.
3. Rajwa, B., Bayraktar, B., Banada, P.P., Huff, K., Bae, E., Hirleman, E.D., Bhunia, A.K., and Robinson, J.P. (2006) Noninvasive forward-scattering system for rapid detection, characterization, and identification of Listeria colonies: image-processing and data analysis. 638105.

4. He, Y., Reed, S., Bhunia, A.K., Gehring, A., Nguyen, L.-H., and Irwin, P.L. (2015) Rapid identification and classification of Campylobacter spp. using laser optical scattering technology. *Food Microbiol.*, **47**, 28–35.
5. Singh, A.K., Sun, X., Bai, X., Kim, H., Abdalhaseib, M.U., Bae, E., and Bhunia, A.K. (2015) Label-free, non-invasive light scattering sensor for rapid screening of Bacillus colonies. *J. Microbiol. Methods*, **109**, 56–66.
6. Kim, K.-P., Singh, A.K., Bai, X., Leprun, L., and Bhunia, A.K. (2015) Novel PCR Assays Complement Laser Biosensor-Based Method and Facilitate Listeria Species Detection from Food. *Sensors*, **15** (9), 22672–22691.
7. Minoni, U., Signoroni, A., and Nassini, G. (2015) On the application of optical forward-scattering to bacterial identification in an automated clinical analysis perspective. *Biosens. Bioelectron.*, **68**, 536–543.
8. Pan, W., Zhao, J., and Chen, Q. (2015) Classification of foodborne pathogens using near infrared (NIR) laser scatter imaging system with multivariate calibration. *Sci. Rep.*, **5** (1).
9. Genuer, V., Gal, O., Méteau, J., Marcoux, P., Schultz, E., Lacot, É., Maurin, M., and Dinten, J.-M. (2016) Optical elastic scattering for early label-free identification of clinical pathogens. *Adv. Biomed. Clin. Diagn. Surg. Guid. Syst. XIV*, **9698**, 96980A.
10. Schultz, E., Genuer, V., Marcoux, P., Gal, O., Belafdil, C., Decq, D., Maurin, M., and Morales, S. (2018) Elastic light scattering for clinical pathogens identification: application to early screening of Staphylococcus aureus on specific medium. *Light-Based Diagn. Treat. Infect. Dis.*, **10479**, 1047909.
11. Tang, Y., Kim, H., Singh, A.K., Aroonnual, A., Bae, E., Rajwa, B., Fratamico, P.M., and Bhunia, A.K. (2014) Light Scattering Sensor for Direct Identification of Colonies of Escherichia coli Serogroups O26, O45, O103, O111, O121, O145 and O157. *PLOS ONE*, **9** (8), e105272.
12. Singh, A.K., Bettasso, A.M., Bae, E., Rajwa, B., Dundar, M.M., Forster, M.D., Liu, L., Barrett, B., Lovchik, J., Robinson, J.P., Hirleman, E.D., and Bhunia, A.K. (2014) Laser

Optical Sensor, a Label-Free On-Plate Salmonella enterica Colony Detection Tool. *mBio*, **5** (1), e01019-13.

13. Kim, H., Rajwa, B., Bhunia, A.K., Robinson, J.P., and Bae, E. (2017) Development of a multispectral light-scatter sensor for bacterial colonies. *J. Biophotonics*, **10** (5), 634–644.
14. Kim, H., Doh, I.-J., Sturgis, J., Bhunia, A.K., Robinson, J.P., and Bae, E. (2016) Reflected scatterometry for noninvasive interrogation of bacterial colonies. *J. Biomed. Opt.*, **21** (10), 107004.
15. Bae, E., Banada, P.P., Huff, K., Bhunia, A.K., Robinson, J.P., and Hirleman, E.D. (2007) Biophysical modeling of forward scattering from bacterial colonies using scalar diffraction theory. *Appl. Opt.*, **46** (17), 3639–3648.
16. Bae, E., Bai, N., Aroonnual, A., Robinson, J.P., Bhunia, A.K., and Hirleman, E.D. (2010) Modeling light propagation through bacterial colonies and its correlation with forward scattering patterns. *J. Biomed. Opt.*, **15** (4), 045001.
17. Kim, H., Doh, I.-J., Bhunia, A.K., King, G.B., and Bae, E. (2015) Scalar diffraction modeling of multispectral forward scatter patterns from bacterial colonies. *Opt. Express*, **23** (7), 8545.
18. Bernard, R., Kanduser, M., and Pernus, F. (2001) Model-based automated detection of mammalian cell colonies. *Phys. Med. Biol.*, **46** (11), 3061.
19. Kim, H., Singh, A.K., Bhunia, A.K., and Bae, E. (2014) Laser-induced speckle scatter patterns in Bacillus colonies. *Front. Microbiol.*, **5**.
20. Huff, K., Aroonnual, A., Littlejohn, A.E.F., Rajwa, B., Bae, E., Banada, P.P., Patsekin, V., Hirleman, E.D., Robinson, J.P., Richards, G.P., and Bhunia, A.K. (2012) Light-scattering sensor for real-time identification of Vibrio parahaemolyticus, Vibrio vulnificus and Vibrio cholerae colonies on solid agar plate. *Microb. Biotechnol.*, **5** (5), 607–620.
21. Maeda, Y., Sugiyama, Y., Kogiso, A., Lim, T.-K., Harada, M., Yoshino, T., Matsunaga, T., Tanaka, T., Maeda, Y., Sugiyama, Y., Kogiso, A., Lim, T.-K., Harada, M., Yoshino, T.,

Matsunaga, T., and Tanaka, T. (2018) Colony Fingerprint-Based Discrimination of Staphylococcus species with Machine Learning Approaches. *Sensors*, **18** (9), 2789.

22. Melter, O., and Radojevič, B. (2010) Small colony variants of Staphylococcus aureus — review. *Folia Microbiol. (Praha)*, **55** (6), 548–558.
23. Simpson, L.M., White, V.K., Zane, S.F., and Oliver, J.D. (1987) Correlation between virulence and colony morphology in Vibrio vulnificus. *Infect. Immun.*, **55** (1), 269–272.
24. Proctor, R.A., Eiff, C. von, Kahl, B.C., Becker, K., McNamara, P., Herrmann, M., and Peters, G. (2006) Small colony variants: a pathogenic form of bacteria that facilitates persistent and recurrent infections. *Nat. Rev. Microbiol.*, **4** (4), 295–305.
25. Enos-Berlage, J.L., and McCarter, L.L. (2000) Relation of Capsular Polysaccharide Production and Colonial Cell Organization to Colony Morphology in Vibrio parahaemolyticus. *J. Bacteriol.*, **182** (19), 5513–5520.
26. Alsulami, T.S., Zhu, X., Abdelhaseib, M.U., Singh, A.K., and Bhunia, A.K. (2018) Rapid detection and differentiation of Staphylococcus colonies using an optical scattering technology. *Anal. Bioanal. Chem.*, **410** (22), 5445–5454.
27. Sousa, A.M., Machado, I., Nicolau, A., and Pereira, M.O. (2013) Improvements on colony morphology identification towards bacterial profiling. *J. Microbiol. Methods*, **95** (3), 327–335.
28. Kim, H., Bai, N., Bhunia, A.K., King, G.B., Hirleman, E.D., and Bae, E. (2013) Development of an integrated optical analyzer for characterization of growth dynamics of bacterial colonies: Integrated optical analyzer for bacterial colony. *J. Biophotonics*, **6** (11–12), 929–937.

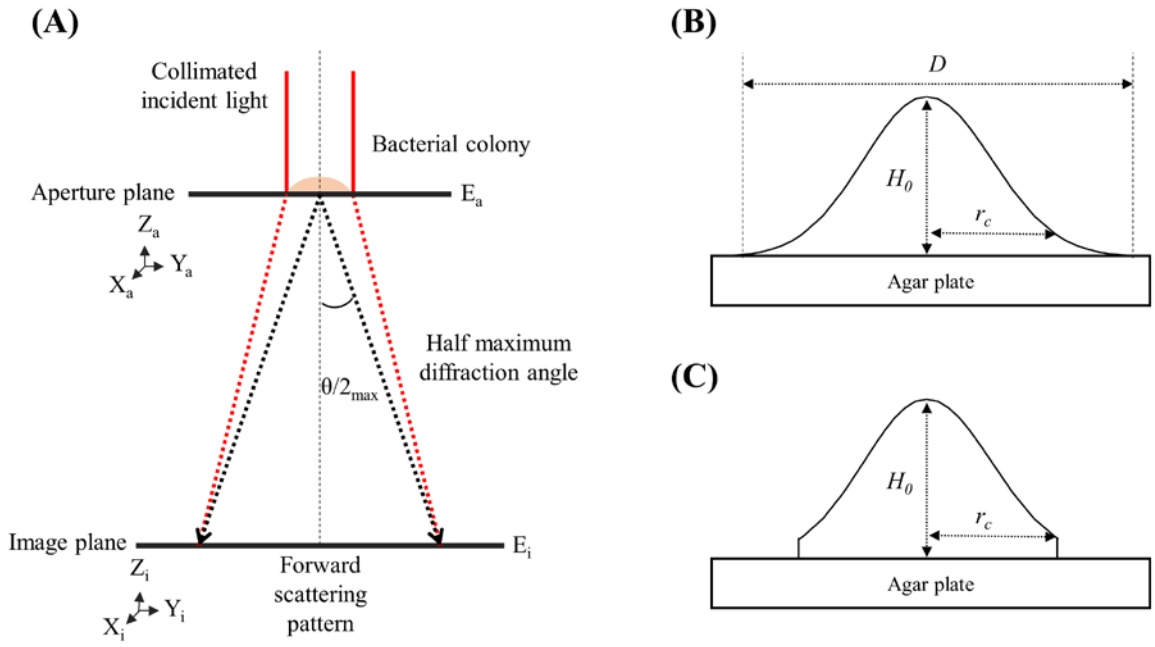

Figure 1: (A) Coordinate definition of the diffraction model based on scalar diffraction theory. (B) Gaussian-profile colony model with tailing edge. (C) Convex-elevation colony model with effective radius.

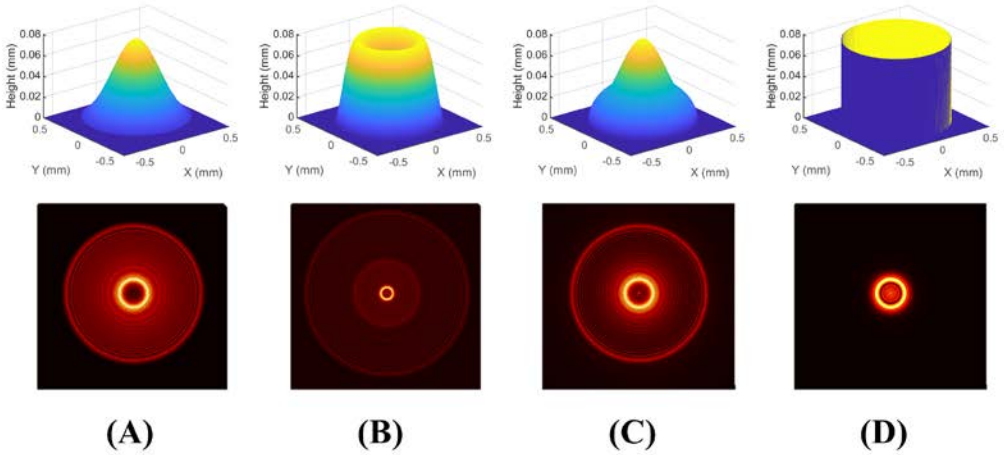

Figure 2. Mathematical model used to generate diverse colony profiles and their associated models. First row displays respective colony models; second shows the simulated diffraction patterns: (A) convex, (B) crateriform, (C) umbonate, and (D) flat.

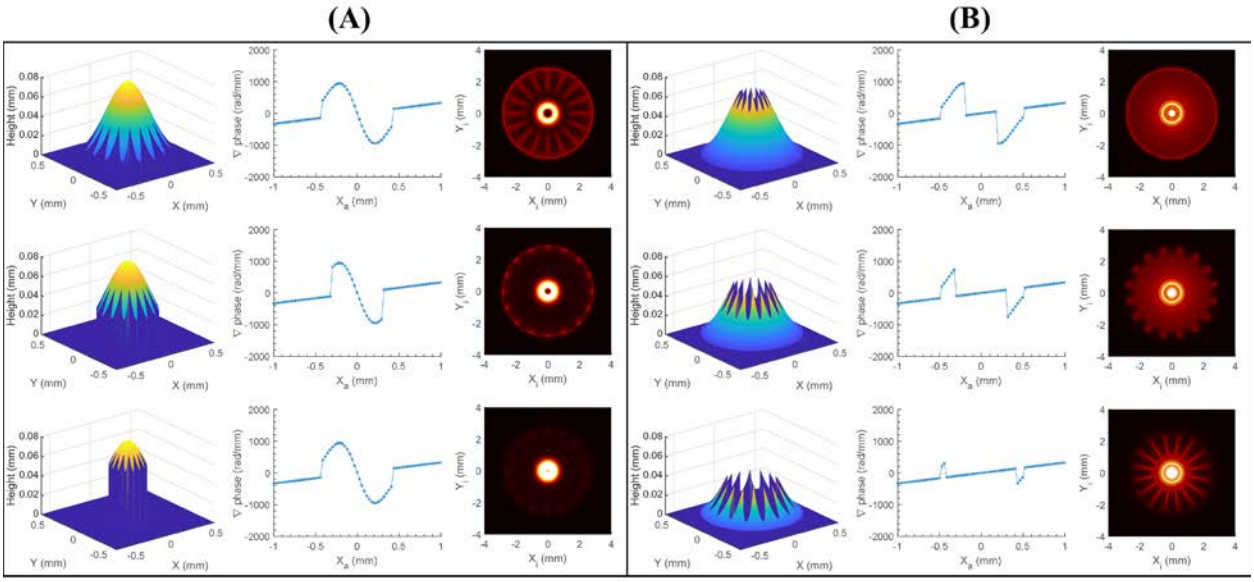

Figure 3: Simulation to explore the effect of the shape of the colony form on the forward scattering patterns. As examples, arbitrary star shape (A) shrinks towards the center or (B) hole is expanding outward. Each column displays a 3-D model (left), the derivative of phase component (middle), and simulated scatter patterns (right).

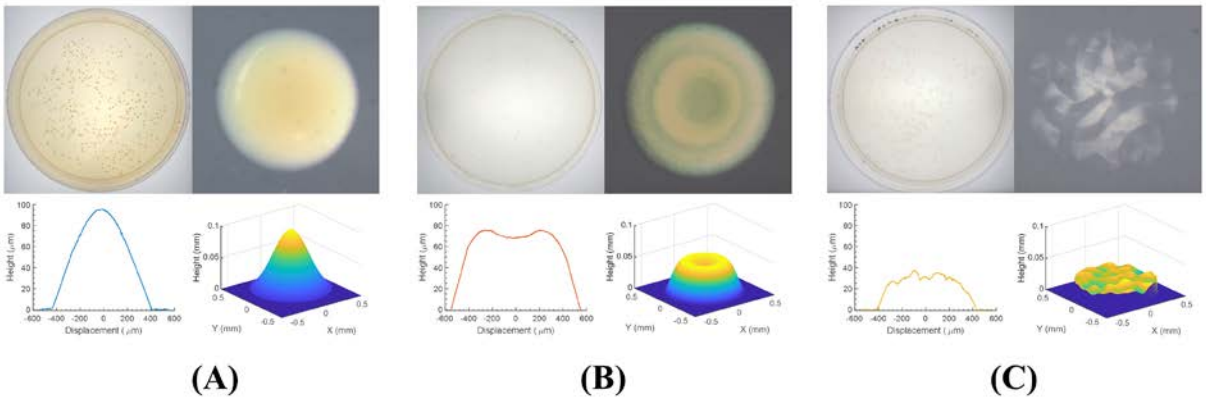

Figure 4: Selected bacteria species for experimental validation. Results are presented counterclockwise, starting from top left, as plate image, single colony image, associated 3-D model, and measured profile. (A) Circular form with convex elevation, *Staphylococcus*. (B) Circular form with crateriform elevation, *Exiguobacterium*. (C) Circular form with flat elevation, *Bacillus*.

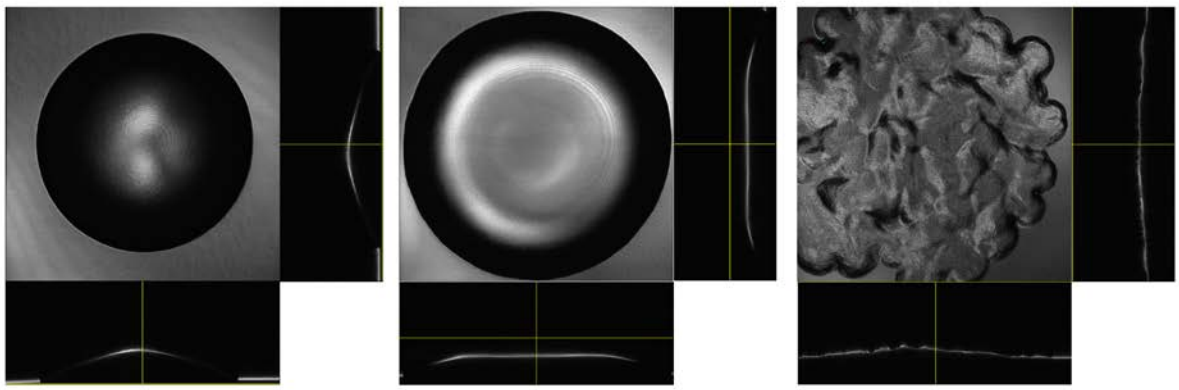

Figure 5: Confocal microscopic images of selected bacterial colonies for validation of theoretical modeling. The orthogonal cross-section profiles are displayed on the right and below the 3D projected confocal image. (A) *Staphylococcus*, (B) *Exiguobacterium*, and (C) *Bacillus.*

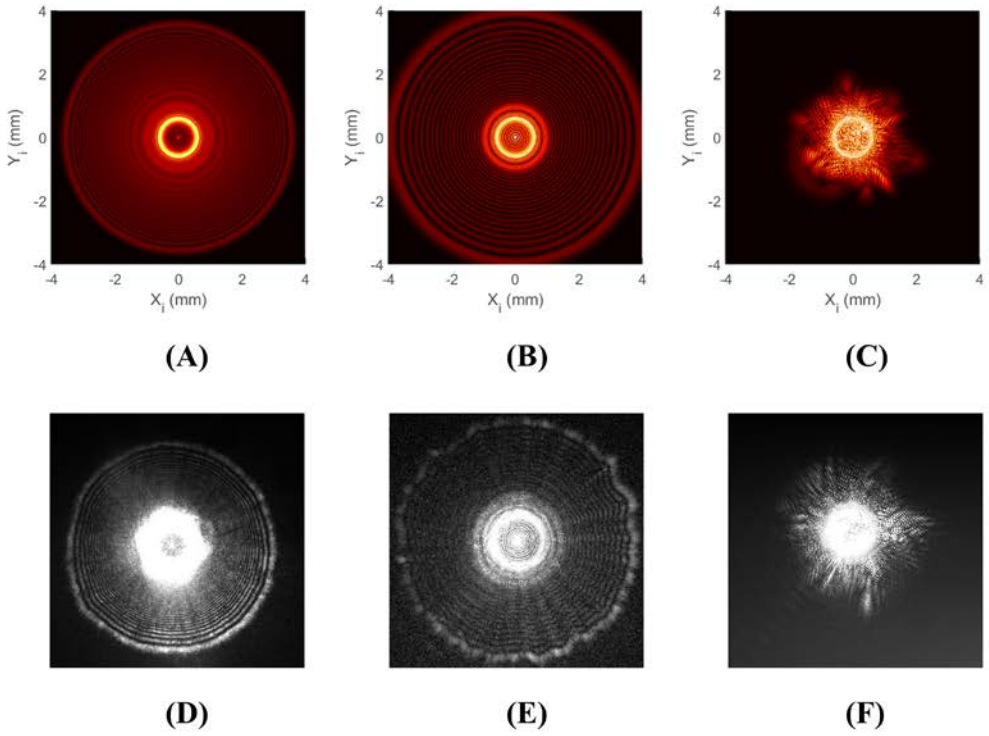

Figure 6: Direct comparison between simulated and experiment patterns for colonies with various elevation. (A), (B), and (C) are simulated diffraction patterns while (D), (E), and (F) are experiment patterns for convex, craiteriform, and flat colonies, respectively.

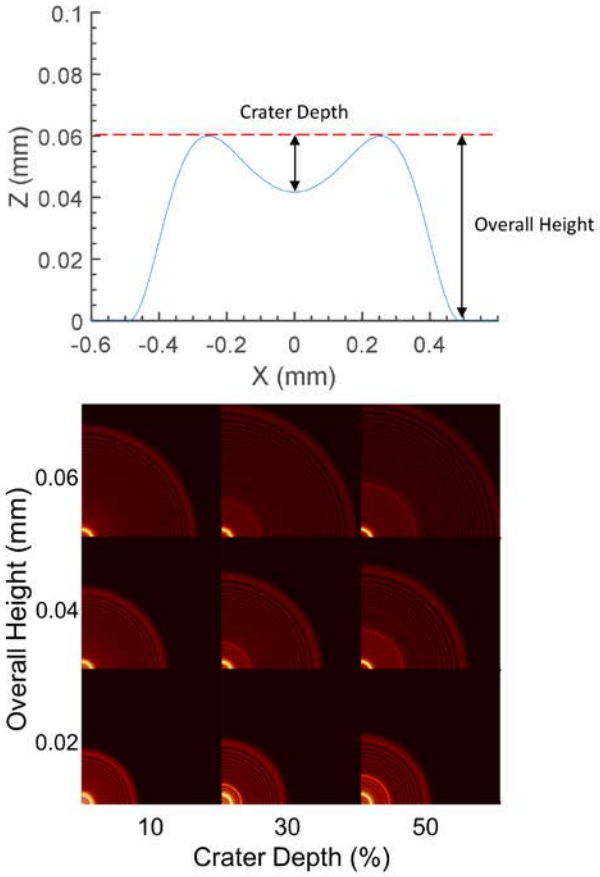

Figure 7: Simulated light-scatter patterns with respect to overall height and crater depth. The definitions of crater depth and overall height are visually described.

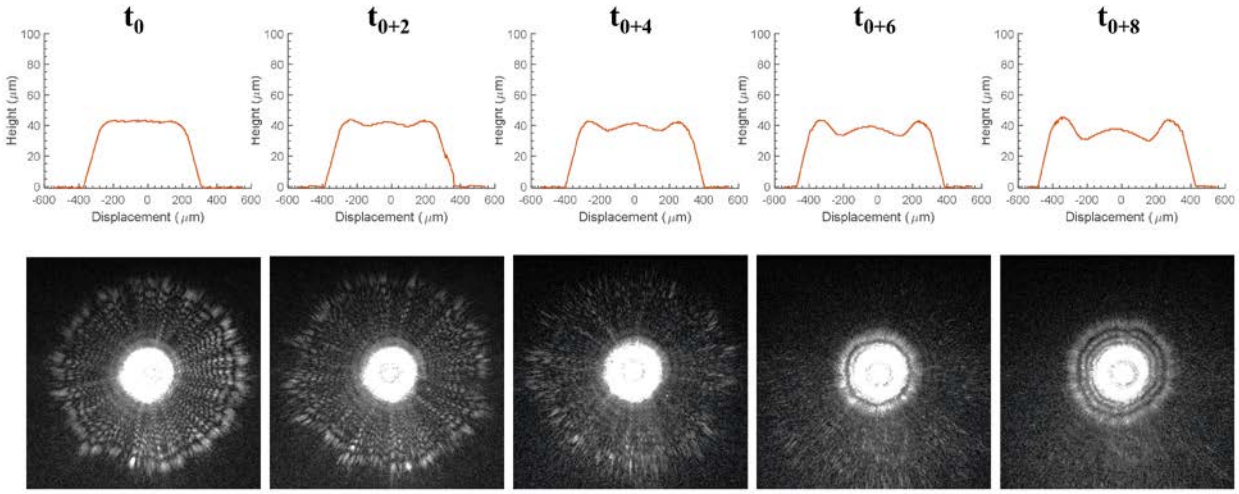

Figure 8: Time-resolved 1-D profiles and light-scatter patterns of *Exigobacterium*, measured from 24 (t_0) to 32 (t_{0+8}) hours. First row: 1-D cross-section profiles; second row: corresponding light-scatter patterns.

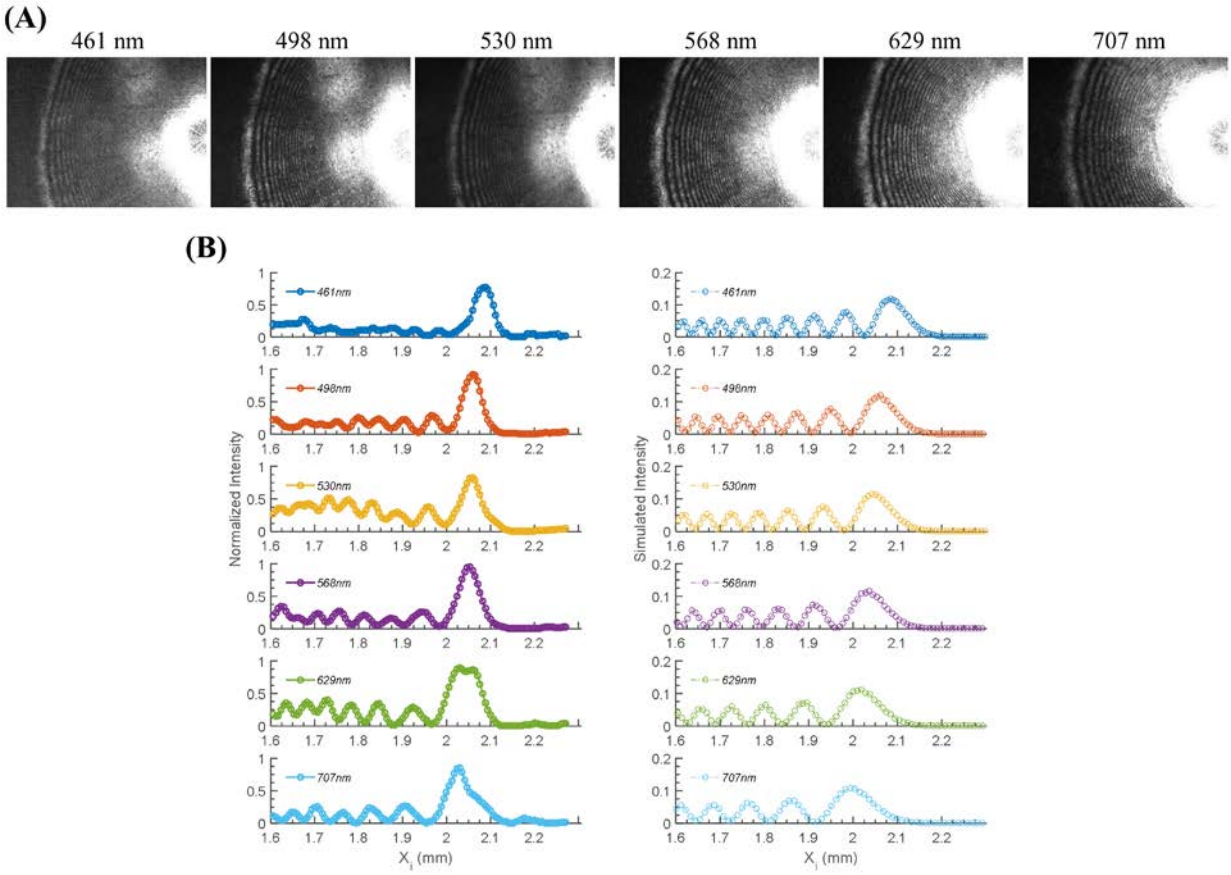

Figure 9: The spectral effect on the shape of scatter patterns. (A) Experiment scatter patterns for *Staphylococcus* based on wavelength change. (B) Cross-section of theoretical (left) and experiment (right) patterns with respect to wavelength change.

Graphical abstract

The forward light scattering pattern generated from a colony with crateriform elevation profile has two differently sized patterns, and the sizes are dependent on the overall height and depth of crater.